



# A New Method for Evaluating the Influence of Coatings on the Strength and Fatigue Behavior of Flexible Glass

Wiebke Langgemach<sup>1</sup> · Edda Rädlein<sup>2</sup>

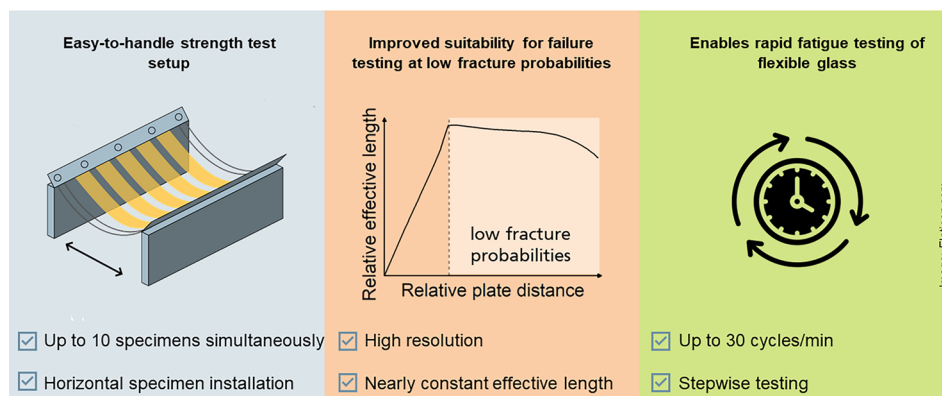
Received: 12 October 2023 / Accepted: 27 February 2024  
© The Author(s) 2024

## Abstract

Flexible glass is an interesting substrate for a variety of displays, especially bendable or foldable ones, as it shows excellent surface properties and appealing haptics. With the necessary skill, flexible glass can be coated with thin films of different functionality, such as electrical or optical thin films, using plasma processes. In displays, thin film coatings such as transparent conductive electrodes and/or antireflective layer stacks are of major importance. Despite its attractive surface properties, however, flexible glass is still brittle, and its strength must be examined and monitored during any functionalization process, especially with regard to the fatigue behaviour. Currently, specific setups for cyclic fatigue testing of coated flexible glass are not available. Therefore, a new test method is presented herein for easy-to-handle rapid strength and fatigue testing using an endurance testing machine. This method overcomes two issues with the commonly used two-point bending test: the correct insertion of specimens is much easier, and both strength and fatigue testing using the same setup are now possible. Finite element method (FEM) simulation outcomes and first experimental simple fracture tests show that results comparable to those with a two-point bending test setup can be achieved with less effort. This makes it possible to analyze the fracture behaviour of flexible glass under cyclic loading and to evaluate the influence of thin film stress and other coating properties on its performance.

## Graphical Abstract

A New Method for Evaluating the Influence of Coatings on the Strength and Fatigue Behavior of Flexible Glass



W. Langgemach, E. Rädlein

Journal of Electronic Materials

**Keywords** Ultra-thin glass · thin film coating · strength testing · reliability · fatigue · U-shape test

Extended author information available on the last page of the article

Published online: 28 March 2024

## Introduction

Over the past few decades, the demand for consumer electronics has increased considerably, leading to significant growth of the display industry. The increasing demand for displays is not limited to consumer electronics but also involves health care and automotive applications as well as other industrial sectors. The growth of the global display market is expected to continue in the coming decade. Indeed, some studies predict an almost doubling of the market value. In addition, these studies anticipate increasing demand for flexible and transparent panel displays.<sup>1</sup> The high demand for functional thin films which are part of display layer stacks is, however, mostly independent of the specific type of display and/or application.

Transparent conductive electrodes are indispensable in almost any kind of display.<sup>2</sup> Thus, the deposition of indium tin oxide as a transparent conductive film for display applications has been studied extensively, for example regarding optimized sputter deposition and process scalability.<sup>3,4</sup> Even though alternatives have been developed and evaluated as well, indium tin oxide on glass or poly(ethylene terephthalate) (PET) clearly dominates the transparent conductive film market today.<sup>5</sup>

In addition to the pure functionality of a display, the deposition of an antireflective layer stack is a typical refinement step to further improve the user experience.<sup>6</sup> Typically, these layer stacks serve other purposes as well, such as providing easy-to-clean properties or scratch protection.<sup>7,8</sup> Since the demand for bendable and flexible displays is increasing, the importance of these multifunctional optical and protective layer stacks will increase as well, as these types of displays are subjected to mechanical loading. This demands not only the adaptation of the thin film properties to the given application but also the careful choice of an adequate substrate.

It is widely acknowledged that flexible glass shows superior material properties to polymer webs for many applications. Flexible glass is transparent in the visible and near-infrared spectrum, and is dimensionally stable, with low surface roughness ( $R_a < 0.5$  nm). Moreover, its barrier properties are outstanding and often used as a benchmark to compare other materials against it. In addition, flexible glass is a suitable substrate for encapsulation. Thus, it is an attractive substrate for display, lighting, and photovoltaic applications.<sup>9</sup> The appealing haptics and the hardness might be additional reasons for the implementation of flexible glass into the first foldable smartphone devices on the market.

However, the brittleness of flexible glass is a major obstacle hindering its widespread use as a serious

alternative to polymer webs. Thus, detailed knowledge about the factors influencing glass strength is necessary to successfully process flexible glass. Early research in the field of glass material science established that the strength of glass is statistically distributed following the Weibull distribution.<sup>10,11</sup> Of course, this is also valid for flexible glass. In addition, there is a relatively small body of literature that deals with flexible glass strength. In general, these studies have all shown that functionalization strongly influences the strength of the glass.<sup>12–14</sup> However, the fatigue behaviour of flexible glass has not yet been studied in detail, and has been neglected in some studies.

Nevertheless, the strength under dynamic loading, i.e. the fatigue behaviour, has much higher practical relevance for ultra-thin glass than for thick glass, since large geometric deformation of flexible glass substrates is possible. This is especially true during the roll-to-roll functionalization processes, where deformations occur intentionally, such as during winding. However, unintentional deformations in production processes can also lead to failure. The strength of thick glass under dynamic loading conditions has been found to be strongly dependent on the loading and surrounding conditions.<sup>15</sup> Obviously, these findings are highly relevant for ultra-thin glass as well. Moreover, due to the higher possible geometric deformation, it can be assumed that detailed knowledge regarding both the strength and fatigue behaviour of flexible glass might be necessary to enable reliable processing with viable production yields. At a minimum, the correlation between these two material properties should be examined.

No standardized test methods are available for either strength or fatigue testing in the characterization of flexible glass. However, a number of techniques has been developed, including two-point bending, (miniaturized) three-point or four-point bending test setups, ball-on-ring-tests, and tensile tests.<sup>14,16–18</sup> The two-point bending test was first described for optical fibres but has since been adopted for flexible glass testing.<sup>19,20</sup>

Despite some disadvantages, the two-point bending test is a universal and simple test setup to determine the strength of flexible glass substrates. Although sometimes called by the same name, the two-point bending test based on Matthewson et al.<sup>19</sup> should not be confused with other test methods such as bending tests on Dynstat test specimens (DIN 53435) or the single cantilever beam test for sandwich composites (ASTM D5528-13). For strength investigation in the two-point bending test based on Matthewson et al.,<sup>19</sup> a specimen is placed horizontally between two vertical plates (or vice versa) and is deformed with decreasing plate distance. It first forms an arc and then turns into a U-shape as soon as wall contact is established (Fig. 1). The strength of the specimen can be calculated from the specimen dimensions and the plate distance

immediately before failure. It is advantageous that this test setup is independent of the specific specimen size. It can be performed equally well for small and large specimens. However, the main disadvantage of this test method is that the effective length of the specimen under tensile load varies during the test. Another major challenge is the precise positioning of the specimen between the two plates. Moreover, this test setup cannot be used for fatigue testing, since normal test machines are not designed for cyclic loading.

To address this problem, a new test setup is proposed herein which is well suited for both strength and fatigue testing of flexible glass. This paper first provides a brief overview of the setup. Then, (fracture) mechanical details are discussed. The final section examines the

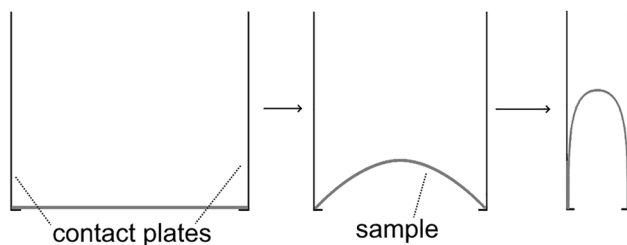


**Fig. 1** Deformation of a sample in a two-point bending test.

comparability between the proposed test setup and a conventional two-point bending test and then describes a fatigue testing procedure for flexible glass.

## Methodology

### Strength and Fatigue Testing Setup

For the new test method, the YUASA U-shape folding test machine (Bayflex Solutions) was adapted to the special needs of flexible glass testing (Fig. 2). This endurance test machine includes a stepper motor but no load cell. It is commercially available and used primarily for endurance testing of polymer substrates and polymer-based products.<sup>21</sup>

The deformation of the specimen during loading can be divided into two phases. For testing, the specimens are placed horizontally between the two specimen holders, as shown in Fig. 3 (1), with a plate distance of 121 mm. Then, only one plate is moved while the other one is fixed. The tilt angle is prescribed by two leaf springs connected to both specimen holders. During the first deformation phase, the specimen forms an arc first and later a drop shape without plate contact (2). At a plate distance of 35 mm, the specimen rests on a contact surface and is then deformed into a U-shape (3) during the second deformation phase. The given test setup allows a minimum plate distance of 11 mm. Minimum and maximum distances as well as the point of

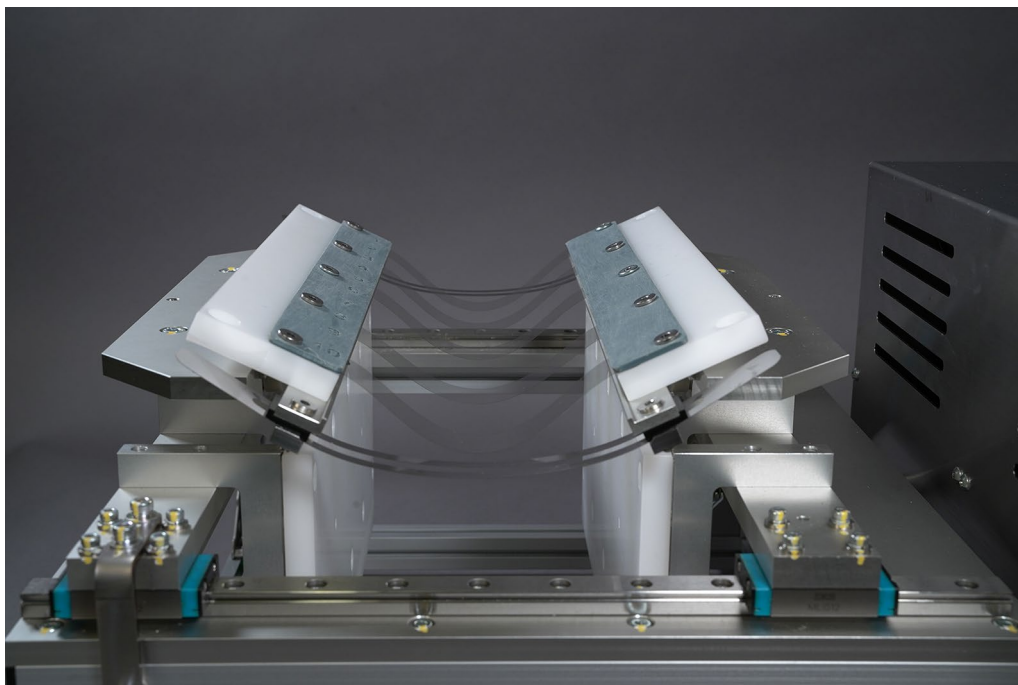


**Fig. 2** U-shape folding test setup with adapted specimen holders (grey) for flexible glass specimens measuring 20 x 120 mm<sup>2</sup>. The right part of the setup is moved while the left part remains fixed.

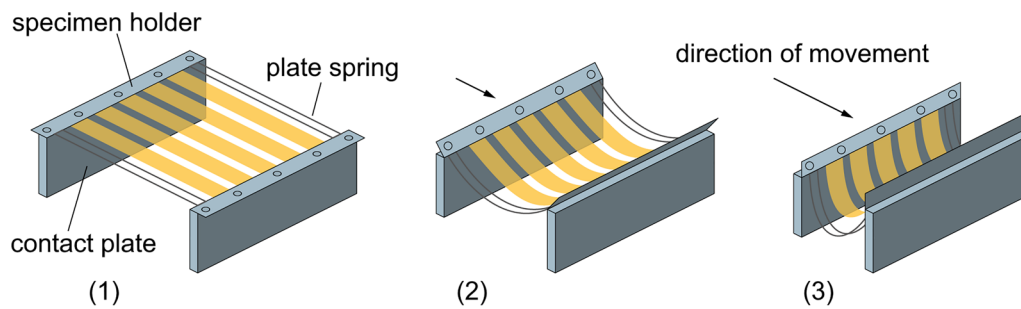


**Fig. 3** Sketch of the specimen deformation during the U-shape folding test. For purposes of clarity, only five specimens are depicted. However, up to ten specimens can be tested simultaneously.

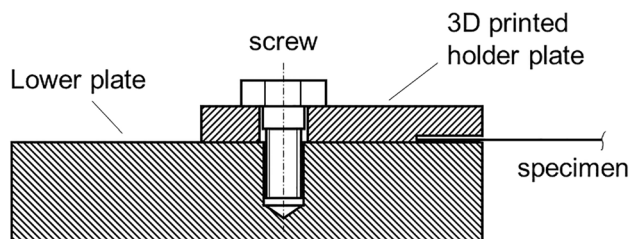


**Fig. 4** Drawing of the specimen holder for the flexible glass substrate as depicted in Fig. 2. The glass substrate is installed with positive locking between the lower white plate and the upper grey 3D-printed holder plate. A slit several micrometer thick between the specimen and the upper holder plate prevents the specimen from breaking.

initiation of plate contact are strongly dependent on the substrate dimensions. Even though polymer substrates and flexible glass might be of similar thickness, the existing substrate holder of the test machine cannot be used for flexible glass testing. For the investigation presented in this paper, flexible glass specimens measuring  $120 \times 20 \text{ mm}^2$  and  $100 \mu\text{m}$  thick were used. Sections measuring  $5 \text{ mm}$  on each side of the specimens were fixed in a specially designed specimen holder.

To avoid glass fracture at the clamping edge, a specially adapted specimen holder was developed. Instead of negative locking, it is based on positive locking of the glass substrates between two plates. This is realized by a small slit between the specimen holder plate of the machine and the customized clamping plate into which the glass substrate is inserted as shown in Fig. 4. As an important benefit, the 3D printed clamping plate allows testing of up to ten specimens simultaneously by providing slits separated from each other by small spacers. However, the most important advantage of this form-fit clamping is that the fixed glass substrates do not undergo pressing even though the two plates are screwed together tightly. Thus, specimens can be deformed once or several times without failure at the clamping edge.

The endurance test machine can be used for regular bending strength tests as well as for fatigue testing. For

bending strength tests, the plate distance is continuously reduced at a speed of  $1 \text{ mm/s}$ . As no load cell is available, the point of fracture is determined acoustically from video recordings of the tests. For fatigue testing of flexible glass, cyclic loading at reasonable speeds of  $20\text{--}30 \text{ cycles/min}$  can be performed. The maximum bending stress is independent of the nature of the test and can be calculated from the plate distance at the moment of fracture.

### Determination of the Stress Distribution in the Specimen

The approximate maximum stress in a flexible glass specimen at a given plate distance can be determined from the measured radius of curvature. For this purpose, a specimen with a highlighted edge was deformed, and the resulting curvature at different plate distances was extracted from frontal photographs (Fig. 5). The bending radius was then measured using an image measurement tool by finding the radius of a circle through three selected points (marked as a triangle) of the deformed specimen.

The strain as a function of curvature and distance from the neutral axis can be related to stress using Hooke's law. The maximum stress  $\sigma_{\text{max}}$  at a given curvature radius  $r$  can be calculated as follows:

$$\sigma_{\text{max}} = \frac{E \cdot t}{2r} \quad (1)$$

The thickness  $t$  is  $100 \mu\text{m}$  and Young's modulus  $E$  is  $74.8 \text{ GPa}$ , as provided in the datasheet for the AF 32 eco ultra-thin glass used (SCHOTT AG).

A simulation using the finite element method (FEM) was conducted to evaluate the validity of the estimate. Since the deformation occurs symmetrically, the problem could be reduced to the simulation of a quarter of the specimen to minimize computational time. The analysis was performed using COMSOL Multiphysics software. Geometric nonlinearity was included, and frictionless contact simulation was performed using the penalty

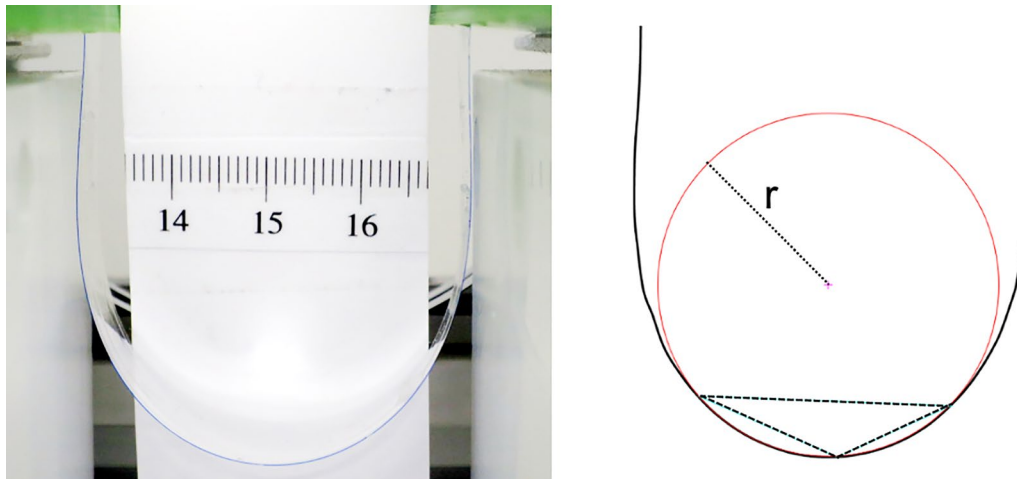


**Fig. 5** Procedure for estimating the maximum stress from the optically determined bending radius. The specimen form was extracted from frontal photographs with a scale. The radius of curvature was

then determined by finding the radius of a circle through three points of the deformed specimen shape.

method. The simulation was conducted for ultra-thin glass (SCHOTT AF 32 eco; SCHOTT AG). Young's modulus was set to 74.8 GPa and Poisson's ratio to 0.24, as provided in the datasheet. The dependence of the tilt angle of the specimen holders on the plate distance was determined from frontal photographs using an image measurement tool. The precision of the measurements was  $\pm 1^\circ$  for tilt angles less than  $45^\circ$  and  $\pm 0.5^\circ$  for larger angles. Since glass is a brittle material, failure due to tensile stress is most likely.<sup>13</sup> Therefore, the first principal stress was used to describe the stress distribution in the specimen.

### Validation Experiments

Validation experiments were carried out to assess whether and how experimental fracture strength data derived from the new U-shape folding test compared with results from two-point bending tests. That is, tests until failure were performed for first evaluations instead of tests under cyclic load. A two-point bending test was carried out using substrates of the same size as in the U-shape test ( $120 \times 20 \times 0.1 \text{ mm}^3$ ). In the U-shape test, 30 individual specimens were tested for each sample set, testing two specimens each simultaneously. The two-point bending tests require greater effort because of the precise positioning of specimens. Thus, only ten specimens were tested for each sample set. Specimens in which no failure occurred throughout the test procedure were excluded from analysis (four specimens of uncoated glass in the U-shape test). The benefit of this approach is that the distribution determined without the survivors describes the region of low failure probability more precisely than a distribution in which surviving specimens are included with a fictive strength

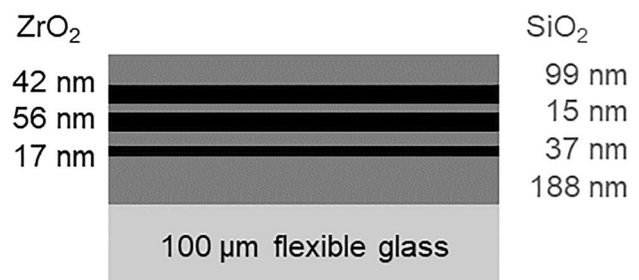


**Fig. 6** Seven-layer antireflective stack with a total thickness of 455 nm that was used as a coating for test evaluation.

above the upper limit of the measurement range. Moreover, the real strength of the survivors is unknown and thus can hardly be considered in calculations.

Both uncoated and coated glass were examined in validation experiments because the test setup should be specifically suitable for testing coated flexible glass in future fatigue tests. In light of the high relevance for industrial applications, a seven-layer antireflective layer stack on 100- $\mu\text{m}$  flexible glass was used (Fig. 6). Silicon dioxide was used as the low refractive material and zirconium dioxide as the highly refractive material. The total thickness of the layer stack was 455 nm. Although the coatings likely influence the mechanical properties of the glass-coating composite, the stress distribution in uncoated glass was used for the investigations using coated samples in this work.

The thin films were deposited by sputter deposition using a vertical inline pilot scale vacuum coater suitable for substrate sizes up to  $1200 \times 600 \text{ mm}^2$ . All thin films were prepared using bipolar pulse DC sputtering. The ZrO<sub>2</sub> layers were deposited using ceramic rotatable targets with

power density of 12.5 kW/m. Pure silicon planar targets with power density of 13.3 kW/m were used for deposition of the SiO<sub>2</sub> layers. The reactive gas control of oxygen was realized using an impedance control loop. The sheet size was 300 × 350 mm<sup>2</sup>. After deposition, the sheets were cut into smaller specimens measuring 20 × 120 mm<sup>2</sup> using a Solid-D cutting blade (MDI Advanced Processing GmbH).

Two variations of the layer stack, referred to as A and B, were deposited on two different glass types (1 and 2). The resulting stacks differed in mechanical thin film stress. These specimens were tested in the U-shape test with the coated/cut side under tensile stress. Forty-five-micrometer polypropylene adhesive tape was attached to the other side of the specimens to reduce the risk of damage caused by glass splinters and to allow for analysis of the fracture patterns after failure. Comparative tests between specimens with and without adhesive tape have shown that the tape lowers the critical strength, while the Weibull modulus of the strength distributions is comparable. Thus, the strength determined with adhesive tape can be seen as a lower estimation of the “real” strength. Nevertheless, only results obtained with comparable adhesive tapes should be compared. Since neither the glass properties nor the specific coating properties are the subject of this paper, the results will only be discussed with respect to the comparison of the two test methods.

Statistical tests were used to determine differences between the sample sets tested with the two test methods. The significance level  $\alpha$  was set to 0.05, i.e. the probability of mistakenly rejecting a true null hypothesis (type I error) was 5%. Based on the results of the normal distribution tests (Ryan–Joiner, comparable to Shapiro–Wilk), suitable tests for variance equality were chosen (Levene,  $F$ -test). Then, the comparison of mean or median values was conducted using a  $t$ -test or a Mann–Whitney test.

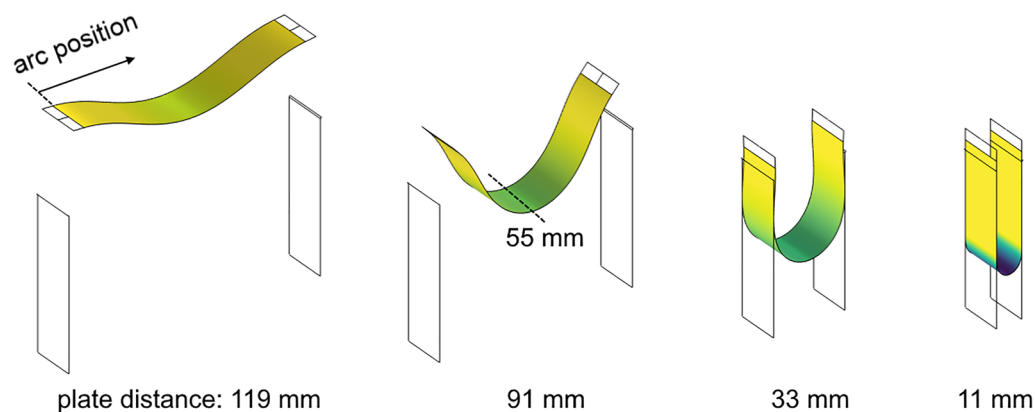


**Fig. 7** FEM simulation of the U-shape folding test for a  $120 \times 20 \times 0.1$  mm<sup>3</sup> flexible glass specimen. The first principal stress of the outer tensile fibres (bottom of the specimen) increases from lighter to darker shading. At a plate distance of 35 mm, contact

## Analysis of Mechanical Characteristics

In the following explanations, the term *arc position* describes the position on the specimen. On each side, the outer 5 mm of the 120-mm-long specimen is used for clamping. Therefore, the arc position ranges from 0 mm to only 110 mm. It can be seen that the maximum stress always occurs in the middle of the specimen, i.e. at an arc position of 55 mm (Fig. 7).

Figure 8 displays the estimated maximum stress using Eq. 1 and the simulated maximum first principal stress as a function of the plate distance. The figure shows the mean value of stress at the arc position of 55 mm, i.e. the whole

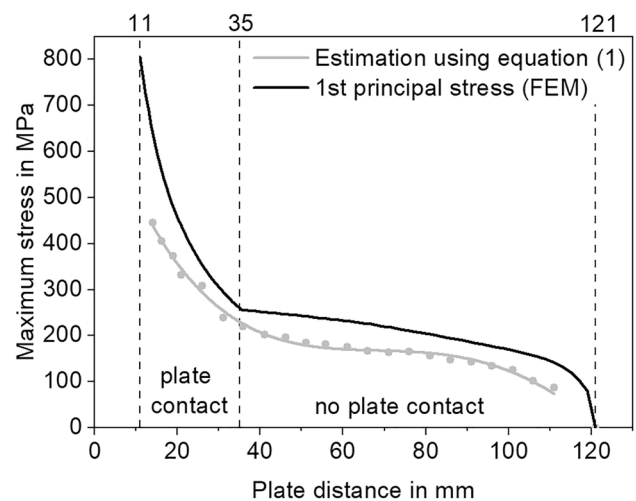


**Fig. 8** Estimated and simulated maximum stress during specimen deformation in the U-shape test. The maximum plate distance is 121 mm, the minimum distance is 11 mm, and contact is established at a distance of approximately 35 mm.

between the specimen and the plate occurs. At 33 mm, first contact is already established. This position is especially interesting concerning the stress profile in the specimen.

axis in the middle of the specimen. In the diagram, the two phases of deformation, *no plate contact* and *plate contact*, can be clearly distinguished. After an initial steep increase in maximum stress, stress increases only slightly until plate contact is established at a plate distance of 35 mm. That is, during the deformation of the horizontal flat specimen into the drop shape, maximum stress only reaches about 250 MPa. However, the maximum stress increases sharply up to 800 MPa at a plate distance less than 35 mm when plate contact is fully established.

The graph shows an underestimation of the maximum stress by the evaluation of bending radii from photographs using Eq. 1. While this underestimation lies in the range of approximately 50 MPa for the phase without plate contact, it increases by a factor of 4 for a plate distance of 11 mm. In general, the discrepancy between estimation and simulation lies in a reasonable range but increases for small plate distances.

The discrepancy between estimation and simulation is partly attributable to the neglecting of transverse effects and superimposed compressive stresses by Eq. 1. That is, Eq. 1 assumes pure bending while the simulation considers the complex deformation determined by the varying tilt angle and the point of establishing contact. Moreover, the FEM simulation considers stress concentration in the vicinity of the specimen edges. Stress is slightly higher at the edge of the specimen, ranging from 8% higher values for a plate distance of 119 mm to 4% for a plate distance of 11 mm. This stress concentration is included in the FEM mean value as displayed in Fig. 8 but is neglected by Eq. 1. Nevertheless, a part of the deviation could also be attributed to measurement errors. In particular for small bending radii, frontal imaging was challenging due to the machine setup, and deviations from the frontal position may have occurred. Moreover, the measurement inaccuracy when determining the radii from the photographs also has an influence, lying in the range of approximately 1 mm. Considering all possible sources of error and inaccuracy, the simulation results are preferable to the estimation for determining the maximum stress from the plate distance at fracture. Since the maximum stress shows nonlinear behaviour, nonlinearity is also expected for the stress distribution in the specimen along its arc length.

The stress profile is highly nonlinear, and the loaded specimen zone decreases as soon as plate contact is established. Figure 9 provides the transverse first principal stress profiles of a flexible glass specimen for three different plate distances. At a plate distance of 119 mm, no contact is established. Even though the substrate curvature is concave and convex at that plate distance (see Fig. 7), a large part of the specimen is considered stress-free in the diagram. This is because the first principal stress does not consider compressive stress. However, considerable stress is present at the clamping edge (approximately 70 MPa, von Mises

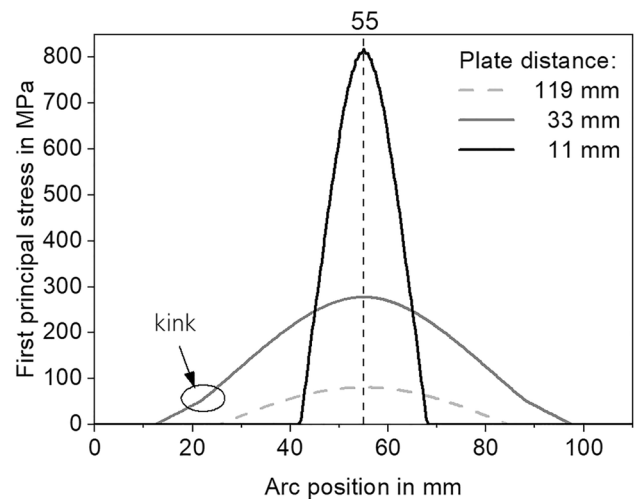


**Fig. 9** Resulting first principal stress curve in a specimen at different plate distances as depicted in Fig. 7. At a plate distance of 119 mm, there is no plate contact and low stress. At 33 mm plate distance, contact to the side walls is freshly established after the initial contact at a distance of 35 mm. This is visible as a slight kink in the curve. At a plate distance of 11 mm, the majority of the specimen is in plate contact, resulting in zero stress in those regions.

stress). Nevertheless, the clamping stress is not relevant for failure since flexible glass with good edge quality seems to have minimum strength of approximately 100 MPa.<sup>12</sup> This non-displayed compressive stress is still relevant at a plate distance of 33 mm. There, plate contact is freshly established. However, a slight kink in the stress curve is the only hint of the drastically changing loading conditions. In contrast, stress clearly peaks for the plate distance of 11 mm when a considerable portion of the specimen is in plate contact and thus actually stress-free. This change between *no plate contact* and *plate contact* strongly influences not only the stress distribution in the specimen but also the resulting effective volume  $V_{\text{eff}}$  under tensile load:

$$V_{\text{eff}} = \int_{\sigma > 0} \left( \frac{\sigma(\vec{r})}{\sigma_r} \right)^m dV \quad (2)$$

where  $\sigma_r$  describes a reference stress that can be arbitrarily chosen but is usually set to  $\sigma_{\text{max}}$ , and  $m$  is the Weibull modulus,<sup>22</sup> which is a dimensionless parameter used to describe the form of a specific Weibull distribution. The general equation of a two-parameter Weibull distribution is given in Eq. 3, where  $F$  is the failure probability and  $\sigma_{\text{crit}}$  the critical strength, i.e. 63.2% of the distribution.<sup>10</sup>

$$F(\sigma) = 1 - e^{-\left(\frac{\sigma}{\sigma_{\text{crit}}}\right)^m} \quad (3)$$

For calculations in this paper, the effective volume was converted to the effective length  $l_{\text{eff}}$  since the cross-section

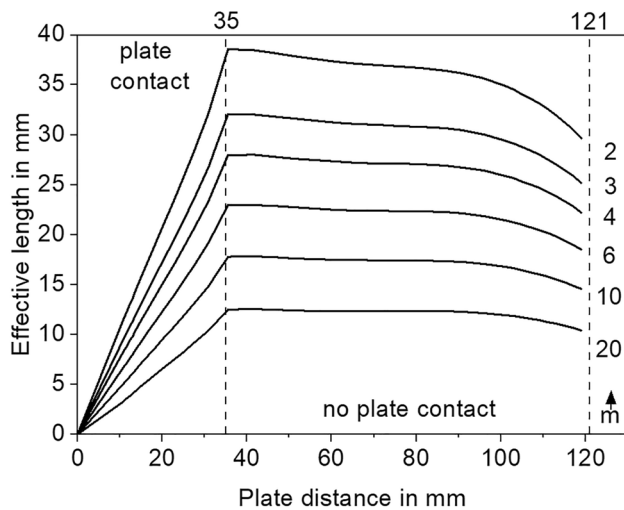


**Fig. 10** Effective length of a specimen in the U-shape folding test as a function of the Weibull modulus  $m$  of the given strength distribution of the sample.

of the specimen is constant. Moreover, the maximum stress  $\sigma_{\max}$  was chosen as the reference stress:

$$l_{\text{eff}} = \int_{\sigma > 0} \left( \frac{\sigma(l)}{\sigma_{\max}} \right)^m dl \quad (4)$$

The effective length of a specimen in the U-shape folding test was calculated based on Eq. 4 using the trapezoidal rule for numerical integration. The effective length remains nearly constant in the relevant range of the phase without plate contact but decreases rapidly when plate contact is established. The specimen area under load then decreases rapidly. As shown in Fig. 10, the decrease is nearly linear as soon as plate contact is established.

Moreover, the effective length of a given specimen is dependent not only on the test setup but also on the underlying Weibull distribution of the sample set. For a low Weibull modulus, i.e. a wide distribution, the effective length is greater than for a higher Weibull modulus, i.e. a narrow distribution. This is not surprising, because for two distributions with equal critical strength but different Weibull modulus values, the probability of failure at low stress is higher for the wider distribution than for the narrow one. In other words, the probability that a crack will lead to failure when exposed to less than the maximum stress is higher for a wide distribution with a low Weibull modulus. It has been shown that the Weibull modulus of flexible glass strength distribution is usually low, e.g. in the range of 3.<sup>12</sup>

As might be expected, the curve of the effective length for the U-shape test resembles the curve for a normal two-point bending test as soon as plate contact is fully established (Fig. 11). In contrast, the effective length is higher for the range without plate contact. This is advantageous because the detection of critical cracks at low failure probability is

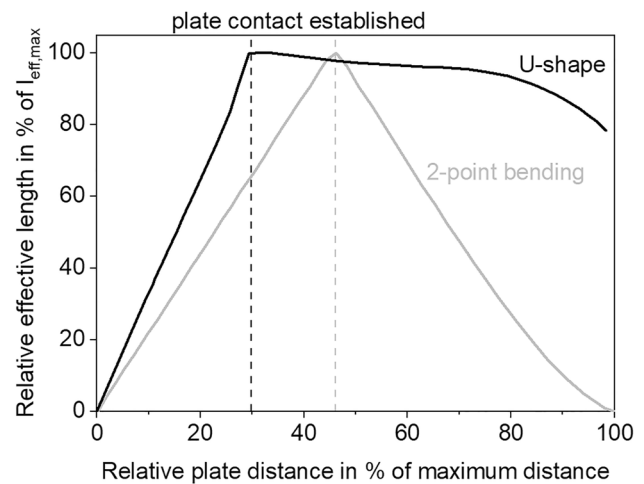


**Fig. 11** Comparison of the relative effective length of a specimen as a function of the relative plate distance in the U-shape test and a two-point bending test (after Jotz<sup>12</sup>) for a Weibull modulus of 3. The specimen size in the two-point bending test was  $50 \times 20 \text{ mm}^2$ .

more likely. In combination with the moderate increase in maximum stress during this phase (Fig. 8), the resolution of the U-shape folding test for failure at low probability is even higher.

The higher effective length compared to a normal two-point bending test in the phase without plate contact is caused by the uncommon deformation shape of the flexible glass in the U-shape folding test. Because of the almost rigid clamping, the free part of the specimen forms a drop shape (see Figs. 2 and 7), leading to a stress distribution where only a small part of the specimen is tensile stress-free (Fig. 9). This is especially valid for small deformations. In contrast, in a normal two-point bending test, stress decreases constantly from the middle of the specimen down to the bearing points, leading to shorter effective length. In addition to this theoretical comparison of the two setups, validation experiments were carried out to compare and contrast the U-shape folding test and the two-point bending test.

## Experimental Validation

All samples were tested with the cut/coated side under tensile stress.

For uncoated glass, the distributions determined in the two test setups were similar. As Fig. 12 illustrates, the data points lie close to each other. The corresponding test results are listed in Table I. Unsurprisingly, no significant difference between the mean values of the two samples could be detected. However, these data must be interpreted with caution because of the small number of specimens in the



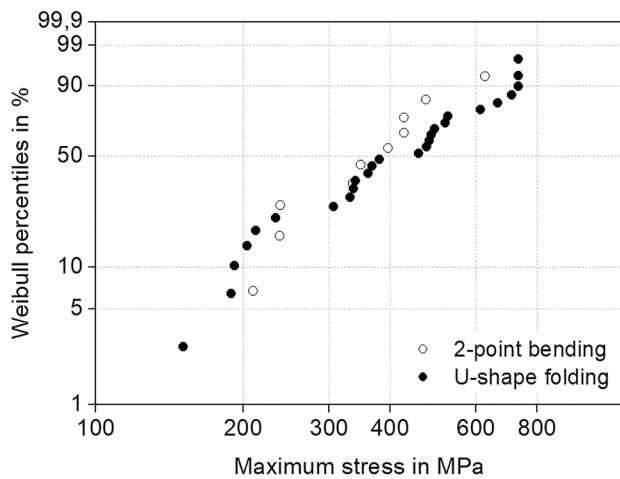


**Fig. 12** Fracture strength of 100-µm uncoated flexible glass as determined by the U-shape folding test and a two-point bending test.

sample of the two-point bending test. To further investigate the correlation between test setups, tests of coated samples were also conducted.

In the case of coated glass samples, most of the distributions derived from the test setups differed from each other in position and slope (Fig. 13). In addition, statistically significant differences were detected for three out of four samples (Table I). In the case of variation (b), the *p* value is at least close to the significance level. Since only ten specimens per sample have been analyzed in the two-point bending test, the significance of the statistical tests is limited. Due to the high effort of two-point bending tests, however, analysis of additional specimens was outside the scope of this paper. In general, based on the simulation and the validation experiments, it seems that the U-shape folding test is an appropriate test setup for strength testing of flexible glass. However, even

though the U-shape test resembles a two-point bending test in the *plate contact* phase, results should not be compared directly with results from two-point bending tests. Since the test is conducted using an endurance test machine, fatigue testing is possible using the same setup.

### Outlook: Fatigue Testing of Flexible Glass

Stepwise testing is necessary to investigate the fatigue behaviour of flexible glass. This is because fatigue testing of glass is challenging for three main reasons.

1. As already discussed, the strength of glass is statistically distributed.<sup>11</sup>
2. Glass fatigue only occurs in a small stress range before failure.<sup>22</sup>
3. The Weibull modulus of the strength distribution of glass objects decreases with a decreasing number and size of defects.<sup>11</sup>

Following from 1 and 2, the fatigue strength of flexible glass is statistically distributed in the same way as the “normal” fracture strength. Moreover, the individual strength values are increasingly scattered with increasing edge length as well as edge and surface quality of a specimen.

In light of the nature of glass strength and the results of this paper, the following procedure is proposed for fatigue testing of flexible glass: In the given setup, ten specimens can be tested at the same time. Thus, three runs of fatigue tests are necessary per sample set. In order to keep the time expenditure low, samples could be tested with 500 cycles at each load step with a speed between 20 and 30 cycles/min. First experiments could be conducted with zero-tension cycles, i.e. with minimum stress of zero. However,

**Table I** Results of the test statistic to compare the samples of the U-shape folding test (U) with samples tested in a two-point bending test (2-PB)

	N		Normal distribution		Variance equality	Comparison of mean/ median values
	U	2-PB	U	2-PB		
Uncoated glass	26	10	Yes	Yes	<i>F</i> -test, <i>p</i> =0.146	<i>t</i> -test, <i>p</i> =0.151
(a) Glass 1 + coating A	30	10	Yes	No	Levene test, <i>p</i> =0.763	MW test, <i>p</i> = <b>0.044</b>
(b) Glass 2 + coating A	30	10	Yes	No	Levene test, <i>p</i> =0.141	MW test, <i>p</i> =0.068
(c) Glass 1 + coating B	30	10	Yes	No	Levene test, <i>p</i> =0.382	MW test, <i>p</i> = <b>0.035</b>
(d) Glass 2 + coating B	30	10	Yes	No	Levene test, <i>p</i> =0.867	MW test, <i>p</i> = <b>0.002</b>

Ryan–Joiner tests were used as normal distribution tests. If the test hypothesis could not be rejected, “yes” is displayed in the table column. “No” indicates a significant deviation from the normal distribution. The Mann–Whitney test (MW test) compares median values, while the *t* test compares mean values. Significant differences between the samples are given in bold. Significance level  $\alpha=0.05$ , *N*=number of specimens.

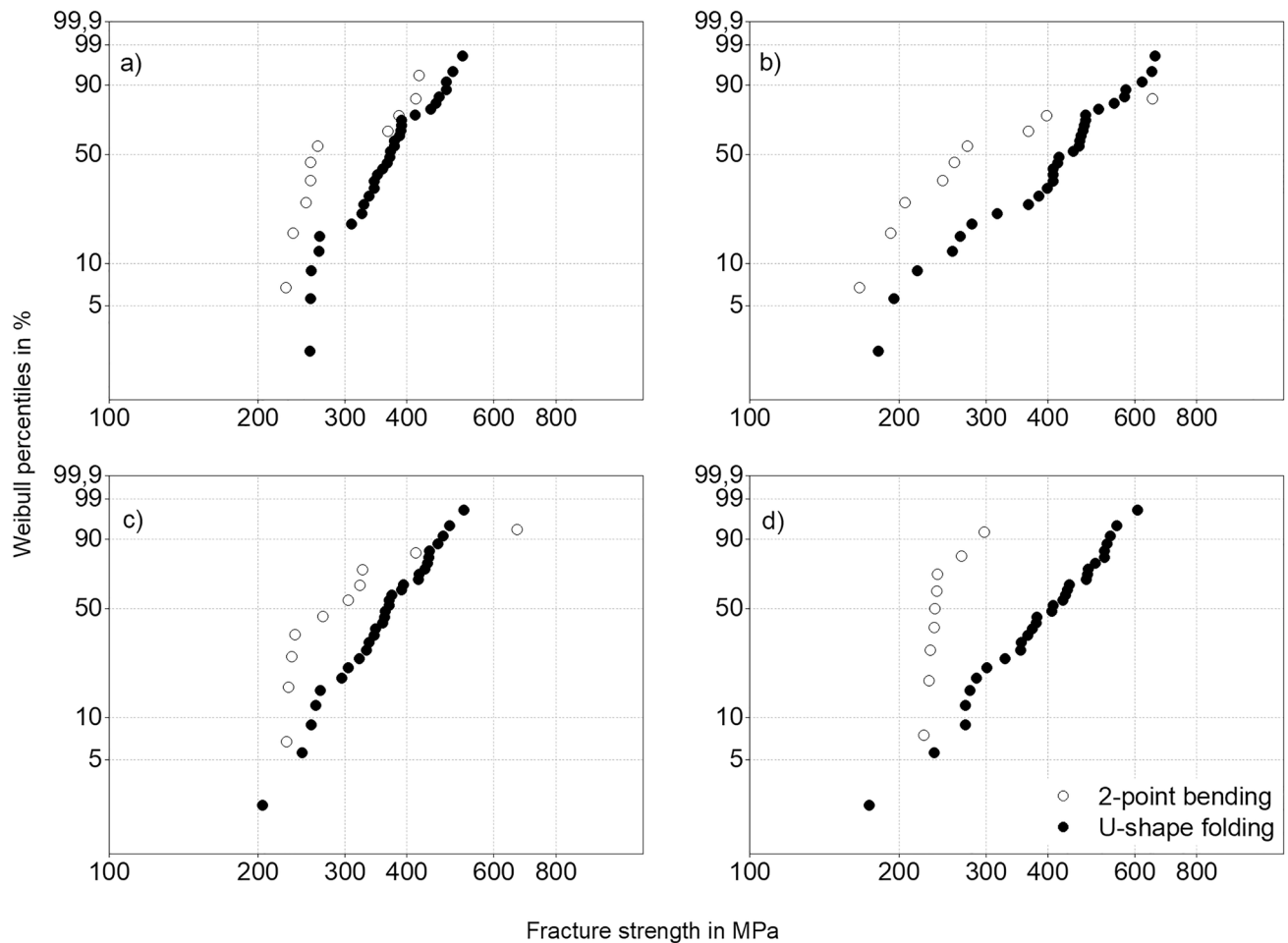


**Fig. 13** Fracture strength of 100- $\mu\text{m}$  coated flexible glass as determined by the U-shape folding test and a two-point bending test. All samples were coated with seven-layer antireflective coatings. Sam-

ples: (a) glass 1 + coating variation A, (b) glass 2 + coating variation A, (c) glass 1 + coating variation B, (d) glass 2 + coating variation B.

tension–tension cycles might also be suitable.<sup>23</sup> After each load step, the load is increased by a specific amount, e.g. 20–30 MPa. For purposes of comparison, the fracture strength of the glass should additionally be determined in the same setup, also with a sample size of at least 30 specimens. Then, by testing the fracture strength of a sample, conclusions can be drawn about the fatigue behaviour which requires greater testing effort.

## Conclusions

Experimental data and simulation results have shown that the U-shape folding test is an appropriate test method to determine the strength of flexible glass. The resolution is especially suitable for the practically relevant failures at low fracture probability. Since the test setup allows cyclic loading without additional effort, fatigue testing of flexible glass is now possible.

It is suggested that stepwise testing be used to find the very narrow fatigue window of flexible glass samples by loading the specimens with a certain number of cycles and then increasing the load by a specific amount. Knowledge regarding the fatigue behaviour of flexible glass—especially after coating—will make it possible to determine suitable processing parameters and thus lower the risk of fracture during functionalization. This could increase the attractiveness of flexible glass for applications beyond foldable displays.

**Acknowledgments** The work presented in this article was funded in part by the AiF-IGF Industrial Collective Research programme on the basis of a decision by the German Bundestag under grant number 21708 BR (project acronym: CUSTOM). This project was supported by the European Society of Thin Films. The authors kindly acknowledge Bayflex Solutions, SCHOTT AG, GfE Fremat GmbH and MDI Advanced Processing GmbH for providing the test machine, flexible glass, sputtering targets and glass cutting services. Moreover, the authors thank the colleagues of Fraunhofer IMWS who conducted the two-point bending tests, and André Weidauer (Fraunhofer IIS) and

Andreas Baumann (Leibniz-Institut für Verbundwerkstoffe GmbH) for helpful comments on the manuscript. Very special thanks go to COM-SOL Multiphysics support, namely Marius Stolz and his colleagues, for substantial support with the FEM simulation.

**Funding** Open Access funding enabled and organized by Projekt DEAL.

**Conflict of interest** The authors declare that they have no conflict of interest.

**Open Access** This article is licensed under a Creative Commons Attribution 4.0 International License, which permits use, sharing, adaptation, distribution and reproduction in any medium or format, as long as you give appropriate credit to the original author(s) and the source, provide a link to the Creative Commons licence, and indicate if changes were made. The images or other third party material in this article are included in the article's Creative Commons licence, unless indicated otherwise in a credit line to the material. If material is not included in the article's Creative Commons licence and your intended use is not permitted by statutory regulation or exceeds the permitted use, you will need to obtain permission directly from the copyright holder. To view a copy of this licence, visit <http://creativecommons.org/licenses/by/4.0/>.

## References

1. M. Vaishnavi, K. Vineet, Display Market, (Allied Market research, 2022) <https://www.alliedmarketresearch.com/display-market>. Accessed: 25 August 2023
2. H.-W. Chen, J.-H. Lee, B.-Y. Lin, S. Chen, and S.-T. Wu, Liquid crystal display and organic light-emitting diode display present status and future perspectives. *Light Sci. Appl.* 7, 17168 (2018).
3. W.J. Lee, Y.-K. Fang, J.-J. Ho, C.-Y. Chen, R.-Y. Tsai, D. Huang, F.C. Ho, H.W. Chou, and C.C. Chen, Pulsed-magnetron-sputtered low-temperature indium tin oxide films for flat-panel display applications. *J. Electron. Mater.* 31, 129 (2002).
4. U. Betz, M. Kharrazi Olsson, J. Marthy, M.F. Escolá, and F. Atamny, Thin films engineering of indium tin oxide large area flat panel displays application. *Surf. Coat. Technol.* 200, 5751 (2006).
5. K. Vineet, Transparent conductive films market. (Allied Market Research, 2022), <https://www.alliedmarketresearch.com/transparent-conductive-films-market>. Accessed: 25 August 2023
6. H.K. Raut, V.A. Ganesh, A.S. Nair, and S. Ramakrishna, Anti-reflective coatings: a critical, in-depth review. *Energy Environ. Sci.* 4, 3779 (2011).
7. D. Glöß, P. Frach, C. Gottfried, S. Klinkenberg, J.-S. Liebig, W. Hentsch, H. Liepack, and M. Krug, Multifunctional high-reflective and antireflective layer systems with easy-to-clean properties. *Thin Solid Films* 516, 4487 (2008).
8. S.B. Khan, H. Wu, X. Huai, S. Zou, Y. Liu, and Z. Zhang, Mechanically robust antireflective coatings. *Nano Res.* 11, 1699 (2018).
9. S. M. Garner, X. Li, and M.-H. Huang, Flexible glass: enabling thin, lightweight, and flexible electronics, ed. by S. M. Garner (John Wiley & Sons, Hoboken, 2017)
10. W. Weibull, A statistical distribution function of wide applicability. *J. Appl. Mech.* 18, 293 (1951).
11. J.E. Ritter, Predicting lifetimes of materials and material structures. *Dent. Mater.* 11, 142 (1995).
12. M. Jotz, Kantenfestigkeitsoptimierte (Weiter-) Entwicklung eines Verfahrens zum Trennen von ultradünnem Glas, 2nd edition (Werkstofftechnik aktuell, Ilmenau 2022)
13. G.S. Glaesemann, *Flexible glass: enabling thin, lightweight, and flexible electronics*. ed. S.M. Garner (Hoboken: Wiley, 2017), p. 35.
14. G. Lorenz, F. Naumann, J. Westphalen, S. Weller, and M. Jungähnel, in 2016 6th Electronic System-Integration Technology Conference (2016), p. 1
15. A.G. Evans, Slow crack growth in brittle materials under dynamic loading conditions. *Int. J. Fract.* 10, 251 (1974).
16. J. Neugebauer, in challenging glass 5 conference (2016), p. 419
17. M. Heiß-Chouquet, K. Nattermann, C. Ottermann, and M. Jotz, Verfahren und Vorrichtung zur Bestimmung der Bruchfestigkeit der Ränder dünner Bahnen sprödbürchigen Materials, German Patent DE 10 2014 110 855 B4 (issued Feb. 2, 2016)
18. M. Heiß-Chouquet, K. Nattermann, and C. Ottermann, Verfahren und Vorrichtung zur Bestimmung der Kantenfestigkeit von scheibenförmigen Elementen aus sprödbürchigem Material. German Patent DE 10 2014 110 856 B4 (issued Feb. 2, 2016)
19. M.J. Matthewson, C.R. Kurkjian, and S.T. Gulati, Strength measurement of optical fibers by bending. *J. Am. Ceram. Soc.* 69, 815 (1986).
20. S. T. Gulati, J. Westbrook, S. Carley, H. Vepakomma, and T. Ono, in SID Symposium Digest of Technical Papers (2011), p. 652
21. Tension-free u-shape folding test, (Yuasa System Co., Ltd., 2023) [https://www.yuasa-system.jp/pdf/DLDMLH-FS\\_DLD-FS\\_en.pdf](https://www.yuasa-system.jp/pdf/DLDMLH-FS_DLD-FS_en.pdf). Accessed: 22 Sept 2023
22. R. Danzer, T. Lube, P. Supancic, and R. Damani, Fracture of ceramics. *Adv. Eng. Mater.* 10, 275 (2008).
23. International Organization of Standardization, *ISO 13003:2003 (E)—Fibre-reinforced plastics—Determination of fatigue properties under cyclic loading conditions* (Geneva: ISO copyright office, 2003).

**Publisher's Note** Springer Nature remains neutral with regard to jurisdictional claims in published maps and institutional affiliations.

## Authors and Affiliations

Wiebke Langgemach<sup>1</sup>  · Edda Rädlein<sup>2</sup>

✉ Wiebke Langgemach  
wiebke.langgemach@fep.fraunhofer.de

<sup>1</sup> Fraunhofer Institute for Organic Electronics, Electron Beam and Plasma Technology FEP, Dresden, Germany

<sup>2</sup> Technische Universität Ilmenau, Ilmenau, Germany